

Section: Astronomy and Meteorology

Frozen orbits around asteroids with zonal gravity, radiation pressure, and third-body perturbations


Ahmed A. Abozaid

Mohamed Radwan

Ahmed H. Ibrahim

Abdelaziz Bakry

Follow this and additional works at: <https://absb.researchcommons.org/journal>

 Part of the [Astrophysics and Astronomy Commons](#)

Frozen Orbits Around Asteroids With Zonal Gravity, Radiation Pressure, and Third-body Perturbations

Ahmed Atyia Abozaid ^{a,*}, Mohamed Radwan ^b, Ahmed Hafez Ibrahim ^a, Abdelaziz Bakry ^a

^a Department of Astronomy and Meteorology, Faculty of Science, Al-Azhar University, Cairo, Egypt

^b Department of Astronomy and Space Science, Faculty of Science, Cairo University, Cairo, Egypt

Abstract

The motion of a probe around asteroids is highly perturbed by several disturbing forces. So, understanding the dynamics in asteroid-proximity environments is essential to designing stable orbits around these small objects. The present work focuses on the effect of a third-body attraction on frozen orbits around asteroids. The full dynamic model includes the asteroid's gravitational field up to the fourth zonal harmonics, and solar radiation pressure, besides a third-body attraction. The work derives semi-analytical solutions of such orbits under the full model perturbations. We carried out several numerical simulations to investigate the effect of the third body on the frozen orbits and the dynamics. We found that the third-body attraction shifts the location of the frozen orbits and affects the dynamics. In addition, we found that the area-to-mass ratio A/m of the probe influences the location of the frozen orbits. Furthermore, we found that the initial eccentricities and inclinations affect the orbits.

Keywords: Asteroids, Frozen orbits, Solar radiation pressure, Third body perturbation

1. Introduction

The subject of frozen orbits has attracted a lot of interest in the field of astrodynamics because of its special stability properties and possible applications in space missions. An orbit that is frozen keeps some orbital elements almost constant over time. Frozen orbits about asteroids are a type of stable orbital motion around irregularly shaped and non-uniformly rotating asteroids. These orbits have minimal variations in their orbital elements, allowing them to persist for long durations without major changes [1,2].

The dynamics of orbits around asteroids differ significantly from those of orbits around more massive bodies that rotate consistently. Because of their complicated rotation and irregular shape, asteroids produce a time-periodic gravitational potential. This means that there is no Jacobi constant and zero-velocity surfaces cannot be used to study the behavior of the system [1]. Utashima identified two types of frozen orbits: one in the asteroid's orbital plane and the other in the solar plane-of-sky,

suitable for smaller asteroids. The study finds that polar orbits have several advantages, including small maintenance fuel requirements. One particularly strong set of frozen orbits is a retrograde family that can reach semi-major axes approximately half the length of the asteroid [2].

Space missions to small objects like comets and asteroids must deal with different perturbations acting on artificial satellites. Using a general perturbative theory of motion, the beginning conditions for these frozen orbits are found by averaging across the argument of node and mean anomaly, which minimizes system complexity while accounting for the gravitational potential up to arbitrary order. This approach can be applied to various celestial bodies, including asteroids like Eros 433 [3].

Because of the characteristics of the frozen orbit, the sectorial harmonic terms were excluded from the frozen orbit design, as they were removed using the averaging technique [4]. Since solar radiation pressure (SRP) can destabilize the orbit at higher radii, it becomes the primary perturbation for spacecraft

Received 9 August 2024; revised 23 September 2024; accepted 26 September 2024.
Available online 14 November 2024

* Corresponding author.
E-mail address: ahmedA.abozaid@azhar.edu.eg (A.A. Abozaid).

<https://doi.org/10.58675/2636-3305.1690>

2636-3305/© 2024, The Authors. Published by Al-Azhar university, Faculty of science. This is an open access article under the CC BY-NC-ND 4.0 Licence (<https://creativecommons.org/licenses/by-nc-nd/4.0/>).

orbiting asteroids, and analytical theories have been developed to characterize its effects and define orbital limitations to ensure stable trajectories. The irregularity of the gravity field of asteroids can have consequences on the orbital stability of satellites, and the influence of SRP and third-body perturbing forces on the stability of orbits around irregularly shaped objects can be determined using several techniques to predict and manage the influences of SRP and third-body forces [5,6].

Jiang et al. [7] examined periodic motions around asteroids 216 Kleopatra and 101955 Bennu, revealing both stable and unstable orbits with complex geometries. Jiang and Baoyin [8] studied periodic orbit families around irregular bodies, identifying multiple bifurcations and proving a conserved quantity that limits the number of periodic orbits at fixed energy levels. Jiang et al. [9] examined orbits and manifolds close to rotating asteroids' equilibrium points, categorizing them into eight scenarios and outlining the submanifold and subspace structures. These investigations shed light on the intricate dynamics of these systems and show the existence of stable orbits close to asteroid surfaces, some as close as half the asteroid's longest dimension.

Over the last decades, researchers have continued to explore more about asteroids, as they give more ideas about our solar system. Moreover, understanding the movement of asteroids gives the perspective of planetary defense to avoid a catastrophic event on Earth by reducing the threat of dangerous asteroids. For example, asteroid Ryugu was visited by Japan's Hayabusa2 spacecraft in 2018 [6,10].

In this paper, we extend the work by Kikuchi et al. [6] and consider the effect of the third-body attraction on the frozen orbits around the Ryugu asteroid. The full dynamical model comprises the asteroid gravity field, the solar radiation pressure, in addition to the third-body attraction.

2. Dynamical model

In this section, we describe the orbital motion of a spacecraft around the asteroid Ryugu. The asteroid is considered as the main central body. The orbital motion of the spacecraft is referenced to an asteroid-centered frame. The spaceship moves around the asteroid under perturbations due to the asteroid's gravity field, solar radiation pressure, and solar gravity (third body). Table 1 lists the asteroid parameters used in this paper.

2.1. Asteroid's gravity field

Assuming that the asteroid is not spherical, then the irregular gravity field of an asteroid can be

Table 1. The properties and physics of asteroid Ryugu [10].

Semi-major axis	$a = 1.190$	AU
Inclination	$i = 5.884$	Degree
Longitude of ascending node	$\Omega = 251.6$	Degree
Argument of perihelion	$\omega = 211.4$	degree
Mean anomaly	$M = 21.94$	degree
Eccentricity	$e = 0.1903$	
Gravitational parameter	$\mathcal{G} m = 30.0 \pm 0.04$	m^3/s^2
Mass	$m = (4.50 \pm 0.06)10^{11}$	kg
Volume	$V = 0.377 \pm 0.005$	km^3
Mean radius	$R_M = 448.31$	m
Maximum radius	$R_{max} = 528.52$	m
Minimum radius	$R_{min} = 377.26$	m
Mean density	$\rho = 1190 \pm 20$	kg/m^3
Mean motion	$N = 1.991 \times 10^{-7}$	s^{-1}

expressed in terms of the orbital elements ($a, e, i, M, \omega, \Omega$) of the probe as [11].

$$R_{As}(a, e, i, M, \omega, \Omega, \theta) = \frac{\mu_{As}}{a} \sum_{n=2}^{\infty} \sum_{m=0}^n \left(\frac{R_{As}}{a}\right)^n \sum_{p=0}^n F_{n,m,p}(i) \times \sum_{q=-\infty}^{\infty} G_{n,p,q}(e) S_{n,m,p,q}(M, \omega, \Omega, \theta), \quad (1)$$

where a denotes the semi-major axis, e the eccentricity, i the inclination, M the mean anomaly, ω the argument of perigee, Ω the longitude of the ascending node, $\mu_{As} = \mathcal{G} m_{As}$ with \mathcal{G} the gravitational constant and m_{As} the mass of the asteroid, R_{As} is the asteroid's radius, and the $F_{nmp}(i)$ and $G_{nmp}(e)$ are the inclination and eccentricity functions [12].

$$F_{nmp}(i) = \sum_{t=0}^{\min(p,k)} \frac{(2n-2t)!}{t!(n-t)!(n-m-2t)!2^{n-2t}} \sin^{n-m-2t}(i) \sum_{s=0}^m \binom{m}{s} \cos^s(i) \sum_{c=0}^n \binom{n-m-2t+s}{c} \binom{m-s}{p-t-c} (-1)^{c-k},$$

$$G_{npq}(e) = (-1)^{|q|} (1 + \beta^2)^n |\beta|^{|q|} \sum_{k=0}^{\infty} P_{npqk} Q_{npqk} \beta^{2k}, \quad (2)$$

where $k = [(n - m) / 2]$, and β being functions of the eccentricity.

$$\beta = \frac{e}{1 + \sqrt{1 - e^2}}$$

$$P_{npqk} = \sum_{r=0}^h \binom{2p' - 2n}{h - r} \frac{(-1)^r}{r!} \left(\frac{(n - 2p' + q')e}{2\beta}\right)^r$$

$$h = k + q', q' > 0; h = k, q' < 0$$

$$Q_{npqk} = \sum_{r=0}^h \binom{-2p'}{h-r} \frac{1}{r!} \left(\frac{(n-2p'+q')e}{2\beta} \right)^r$$

$$h = k, q' > 0; h = k - q', q' < 0$$

When $p' \leq \frac{l}{2}$ then $p' = p; q' = q$, while $p' = l - p; q' = -q$ for $p' > \frac{l}{2}$.

$$S_{nmpq} = \begin{cases} -J_{nm} \text{Cos}(\psi_{nmpq}) \text{ mod } (n - m, 2) = 0, \\ -J_{nm} \text{Sin}(\psi_{nmpq}) \text{ mod } (n - m, 2) = 1. \end{cases}$$

$$\psi_{nmpq} = (n - 2p)\omega + (n - 2p + q)M + m(\Omega - \theta) - m \lambda_{nm}, \tag{3}$$

Now we consider only the long-period dynamics by averaging equation (1) over the fast angles M and θ , (setting $n - 2p + q = 0$, and $m = 0$), then the explicit expansions of R_{AS} up to order $n = 4$ can be written as

$$R_{AS} = \frac{R_{AS}^2 \mu_{AS} J_2}{8a^3(1 - e^2)^{3/2}} (1 + 3 \cos(2i)) + \frac{3e R_{AS}^3 \mu_{AS} J_3}{32a^4(1 - e^2)^{5/2}} (\sin(i) + 5 \sin(3i)) \sin(\omega) - \frac{3R_{AS}^4 \mu_{AS} J_4}{1024a^5(1 - e^2)^{7/2}} \tag{4}$$

$$\times (18 + 27e^2 + 35(2 + 3e^2)\cos(4i) + 200e^2 \cos(2\omega) \sin^2(i) + 20 \cos(2i)(2 + 3e^2 + 14e^2 \cos(2\omega)\sin^2(i))).$$

Where the zonal harmonic coefficients of the gravity field of the asteroid are given as [6]. $J_2 = 3.8727 \times 10^{-2}$, $J_3 = -1.7568 \times 10^{-3}$ and $J_4 = -2.2571 \times 10^{-2}$.

2.2. Solar gravity

Another possible disturbing force is solar gravity, which provides the solar tidal force on a spaceship around the Ryugu asteroid. The perturbation due to the Sun's attraction can be written as an expansion in the orbital elements of the Sun and spaceship, using the following formula [11,13].

$$R_{sun} = \mathcal{G} \mathcal{M} S \sum_{l \geq 2}^2 \sum_{m=0}^l \sum_{p=0}^l \sum_{h=0}^l \sum_{q=-\infty}^{\infty} \sum_{j=-\infty}^{\infty} \frac{a^l}{a s^{l+1}} K_m \frac{(l-m)!}{(l+m)!} F_{lmp}(i) \tag{5}$$

$$F_{lmh}(is) H_{lpq}(e) G_{lhj}(es) \text{Cos}(\phi_{lmphqj}),$$

$$\phi_{lmphqj} = (l - 2p)\omega + (l - 2p + q)M - (l - 2h)\omega s - (l - 2h + j)Ms + m(\Omega - \Omega s).$$

where MS is the mass of the disturbing body, ($as, es, is, \omega s, \Omega s$) are the orbital elements of the Sun. The functions $F_{lm p}(i)$ and $F_{lmh}(is)$ are the Kaula's inclination functions. The functions $H_{lpq}(e)$ and $G_{lhj}(es)$ represent the Hansen coefficients $X_{l-2p+q}^{l,l-2p}(e)$, $X_{l-2h+j}^{-(l+1),l-2h}(es)$, and can be computed with an algebraic manipulator through the following formula [14,15].

$$X_k^{n,m}(e) = \frac{1}{(1 + \beta^2)^{n+1}} \sum_{s=0}^{s_1} \sum_{t=0}^{t_1} \binom{n-m+1}{s} \times \binom{n+m+1}{t} (-\beta)^{s+t} J_{k-m-s+t}(ke)$$

where n, m, k are integers, J_b denotes the Bessel function of the first kind and s_1, t_1 , are defined by

$$s_1 = \begin{cases} n - m + 1 \rightarrow n - m + 1 \geq 0 \\ \infty \rightarrow n - m + 1 < 0 \end{cases},$$

$$t_1 = \begin{cases} n + m + 1 \rightarrow n + m + 1 \geq 0 \\ \infty \rightarrow n + m + 1 < 0 \end{cases}$$

Expanding equation (5) up to $l = 2$, then

$$R_{sun} = \mathcal{G} \mathcal{M} S \sum_{l=2}^2 \sum_{m=0}^l \sum_{p=0}^l \sum_{h=1}^1 \sum_{j=0}^0 \frac{a^l}{as^{l+1}} K_m \frac{(l-m)!}{(l+m)!} F_{lmp}(i) F_{lmh}(is) H_{lp}(2p-l)(e) \times G_{lhj}(es) \cos \left(\frac{(l-2p)\omega + (l-2p-l+2p)M}{-(l-2h)\omega s - (l-2h)Ms + m(\Omega - \Omega s)} \right), \quad (6)$$

Finally, we have the following expression:

$$R_{sun} = \frac{a^2 \mathcal{G} \mathcal{M} S}{128as^3(1-es)^{3/2}} \left[\begin{array}{l} 30e^2(1+3\cos(2is))\cos(2\omega)\sin^2(i) \\ +(2+3e^2)(1+3\cos(2i))(1+3\cos(2is)) \\ +12(2+3e^2)\cos(\Omega-\Omega s)\sin(2i)\sin(2is) \\ +12(2+3e^2)\cos(2(\Omega-\Omega s))\sin^2(i)\sin^2(is) \\ +120e^2\cos^4(i/2)\cos(2(\omega+\Omega-\Omega s))\sin^2(is) \\ +120e^2\sin^4(i/2)\cos(2(\omega-\Omega+\Omega s))\sin^2(is) \\ -120e^2(1+\cos(i))\cos(is)\cos(2\omega+\Omega-\Omega s)\sin(i)\sin(is) \\ -120e^2(-1+\cos(i))\cos(is)\cos(2\omega-\Omega+\Omega s)\sin(i)\sin(is) \end{array} \right]. \quad (7)$$

2.3. Solar radiation pressure

The motion of a spaceship in the vicinity of an asteroid is strongly perturbed by solar radiation pressure. Particularly when the asteroid has weak self-gravity and in the case of a spaceship with a large area-to-mass ratio. The potential function of the SRP can be written as [11].

$$R_{srp} = -C_r P_r \frac{A}{\mathcal{M}} \sum_{l=1}^1 \sum_{m=0}^l \sum_{p=0}^l \sum_{h=0}^l \sum_{q=-\infty}^{\infty} \sum_{j=-\infty}^{\infty} \frac{a^l}{as^{l+1}} K_m \frac{(l-m)!}{(l+m)!} F_{lmp}(i) \quad (8)$$

$$F_{lmh}(is) H_{lp}(e) G_{lhj}(es) \cos(\phi_{lmp h q j}),$$

Where A/\mathcal{M} (β) is the area-to-mass ratio of the spacecraft, C_r is the reflectivity coefficient, P_r and is the SRP for Earth.

$$R_{srp} = -C_r P_r \frac{A}{\mathcal{M}} \sum_{l=1}^1 \sum_{m=0}^l \sum_{p=0}^l \sum_{h=0}^l \sum_{j=0}^0 \frac{a^l}{as^{l+1}} K_m \frac{(l-m)!}{(l+m)!} F_{lmp}(i) F_{lmh}(is) H_{lp}(2p-l)(e) \times G_{lhj}(es) \cos \left(\frac{(l-2p)\omega + (l-2p-l+2p)M}{-(l-2h)\omega s - (l-2h)Ms + m(\Omega - \Omega s)} \right), \quad (9)$$

The expression for the corresponding disturbing potential is given by

$$R_{srp} = -\frac{3ae\left(1 - \frac{e_s^2}{2}\right)A}{8\mu} \begin{pmatrix} 2 \sin(i) \sin(is) \cos(Ms + \omega + \omega_s) \\ -2 \sin(i) \sin(is) \cos(Ms - \omega + \omega_s) \\ -(1 - \cos(i))(1 - \cos(is)) \cos(Ms - \omega + \Omega + \omega_s - \Omega_s) \\ -(1 + \cos(i))(1 - \cos(is)) \cos(Ms + \omega + \Omega + \omega_s - \Omega_s) \\ -(1 + \cos(i))(1 + \cos(is)) \cos(Ms - \omega - \Omega + \omega_s + \Omega_s) \\ -(1 - \cos(i))(1 + \cos(is)) \cos(Ms + \omega - \Omega + \omega_s + \Omega_s) \end{pmatrix} C_r P_r. \quad (10)$$

3. The equations of motion

To analyze the influence of the perturbing functions on the orbital elements of the probe, we introduced the normalized potential into Lagrange planetary equations. This system of equations describes the time variation of the orbital elements. The temporal evolutions of the eccentricity and argument of perigee are given by their corresponding Lagrange planetary equations. These equations can be written as [16].

$$\frac{da}{dt} = \frac{2}{na} \frac{\partial U}{\partial M}, \quad (11.1)$$

$$\frac{de}{dt} = \frac{1 - e^2}{na^2e} \frac{\partial U}{\partial M} - \frac{\sqrt{1 - e^2}}{na^2e} \frac{\partial U}{\partial \omega}, \quad (11.2)$$

$$\frac{di}{dt} = \frac{\cos(i)}{na^2\sqrt{1 - e^2}\sin(i)} \frac{\partial U}{\partial \omega} - \frac{1}{na^2\sqrt{1 - e^2}\sin(i)} \frac{\partial U}{\partial \Omega}, \quad (11.3)$$

$$\frac{d\Omega}{dt} = \frac{1}{na^2\sqrt{1 - e^2}\sin(i)} \frac{\partial U}{\partial i} - N, \quad (11.4)$$

$$\frac{d\omega}{dt} = \frac{\sqrt{1 - e^2}}{na^2e} \frac{\partial U}{\partial e} - \frac{\cos(i)}{na^2\sqrt{1 - e^2}\sin(i)} \frac{\partial U}{\partial i}, \quad (11.5)$$

Where $n = \sqrt{\mu/a^3}$ is the mean motion of the spacecraft. The Lagrange planetary equations are modified by subtracting the spin rate N from the node, ($\Omega = \tilde{\Omega} - N$), defining the node relative to the sun line. The averaged perturbing function U is given by the following:

$$U = R_{As} + R_{sun} + R_{srp} \quad (12)$$

4. Frozen orbits results

Artificial satellites around the Earth experience important variations in their orbital elements due to perturbing forces. Consequently, the control process for long-range missions requires continuous maintenance. However, carefully selecting the orbital elements can reduce the number of corrective maneuvers. By designing the mission such that the mean eccentricity and argument of pericenter remain constant on average, we ensure a longer lifetime for the spacecraft. In the case of a spacecraft orbiting a small body (asteroid), the situation is more complicated. This is because the magnitudes of the disturbing forces can be different from the planetary orbiter case. In the present case, we consider that the small body gravity field will dominate over the included perturbing forces.

To compute the frozen orbits, we first eliminate the short-period terms from the disturbing function of the problem. Afterward, the normalized disturbing function is introduced into the Lagrange planetary equations to obtain the secular variations of e and ω . Setting these equations (equation (11)) to zero, frozen orbits around asteroid Ryugu are identified as the equilibria of these equations. The definition of frozen orbits can be written in the form

$$\frac{da}{dt} = 0, \frac{di}{dt} = 0, \frac{de}{dt} = 0, \frac{d\omega}{dt} = 0, \frac{d\Omega}{dt} = 0. \quad (13)$$

we take the case $\cos \Omega = 0$ and $\sin \omega = 0$, then

$$\begin{aligned}
\frac{d\omega}{dt} = & \frac{3 \mathcal{E} \mathcal{M} S}{16as^3 \sqrt{1-e^2} (1-es)^{3/2} \sqrt{\frac{\mu}{a^3}}} (\cos^2(i) + 4e^2 \cos^2(i) + 3(1+4e^2)\cos^2(i)\cos 2(is) + \frac{1}{4}(-1+e^2)(16+48\cos 2(is) \\
& -3\cos 2(is-\Omega s) + 6\cos 2(\Omega s) - 3\cos 2(is+\Omega s))\sin^2(i) + 2\cos^2(i)\cos(2\Omega s)\sin^2(is) \\
& + 8e^2 \cos^2(i)\cos 2(\Omega s)\sin^2(is) - \frac{1}{4}(-1+e^2)(-24+5\cos 2(i-\Omega s) + 30\cos 2(\Omega s) + 5\cos 2(i+\Omega s))\sin^2(is) \\
& - 2(1+4e^2)\cos(2i)\cot(i)\sin 2(is)\sin(\Omega s) - 4(-1+e^2)(1+2\sin 2(i)\sin 2(is)\sin(\Omega s))) \\
& + \frac{3A(-2+es^2)}{8ae\sqrt{1-e^2} \mathcal{M} \sqrt{\frac{\mu}{a^3}}} (2(-1+e^2)\sin(i)\sin(is)\sin(Ms+\omega s) + \cos(i)(-(-1+\cos(is))\cos(Ms+\omega s-\Omega s) \\
& + (1+\cos(is))\cos(Ms+\omega s+\Omega s) + 2e^2 \cot(i)\sin(is)\sin(Ms+\omega s))) \quad C_r P_r \\
& + \frac{1}{2048a^4 e(-1+e^2)^4} 3R^2 \sqrt{\frac{\mu}{a^3}} \csc(i) (128a^2 e(-1+e^2)^2 (\sin(i) + 5\sin 3(i))J_2 + R(32a(-1+e^2) \\
& (-1-3e^2-4\cos 2(i) + 5(1+7e^2)\cos 4(i))J_3 - 10eR(96+145e^2+4(48+77e^2)\cos 2(i) \\
& + 7(32+45e^2)\cos 4(i))\sin(i)J_4))
\end{aligned} \tag{14}$$

Frozen orbits are obtained when Equation (14) vanish i.e.

$$\frac{d\omega}{dt} = 0. \tag{15}$$

Solving equation (15), we obtain an equation that depends on the set of variables (a, i, e) . This equation can be represented as a three dimensional surface. Points on this surface are the equilibrium points of the dynamic system, i.e. frozen orbits. In the literature, researchers used several criteria to illustrate and characterize these orbits. Among them is the eccentricity–vector diagram which is used to visualize a set of frozen solutions. To nullify the argument of pericenter variation, Figs. 1–4 depict the location and behavior of frozen orbits in the (i, e) , and (a, i) spaces. We used initial conditions in the range, $a \in [1, 5] \text{ km}$, $e \in [0, 0.9]$, and $i \in [0^\circ, 180^\circ]$. The results are analyzed using different combinations of disturbing functions. Figure 1a illustrates the frozen orbits under perturbations due to the asteroid's gravity field, the solar radiation pressure, and the third body. Figure 1b illustrates the frozen orbits where the effect of the third body is ignored. We notice the shift in the locations of frozen orbits between the two plots. This is due to the presence of the third-body effect. We also observe the

significance of the semi-major axis on the locations of frozen orbits in both cases. Furthermore, we notice that some of the frozen orbits present in the case of the full model disappear from Fig. 1b.

Figure 2 depicts the behavior of the frozen orbits in the (i, e) space with fixed semi-major axis, $a = 5 \text{ km}$, and different values of β . We used two models, the blue color represents the model that comprises the asteroid's gravity field plus the solar radiation pressure, whereas the red color represents all perturbations (full model). Figure 2a describes the orbits when $\beta = 0.024$, while in Fig. 2b $\beta = 0.24$. We observe in both models that the parameter β shifts the location of the frozen orbits.

Figure 3 shows the plan of the frozen orbit in the (a, i) space with fixed $\beta = 0.024$, and different eccentricity values. In Fig. 3a all the disturbing functions are considered, while in Fig. 3b the effect of the third body is ignored. We observe that, in both models, changing the eccentricity leads to a shift in the location of the frozen orbits.

Figure 4 depicts the contour maps (a, i) , with $e = 0.9$ and different β values. Figure 4a describes the orbits when $\beta = 0.024$, while in Fig. 4b $\beta = 0.24$. The blue color represents the model comprising the asteroid's gravity field besides the solar radiation pressure, while the red represents all perturbations.

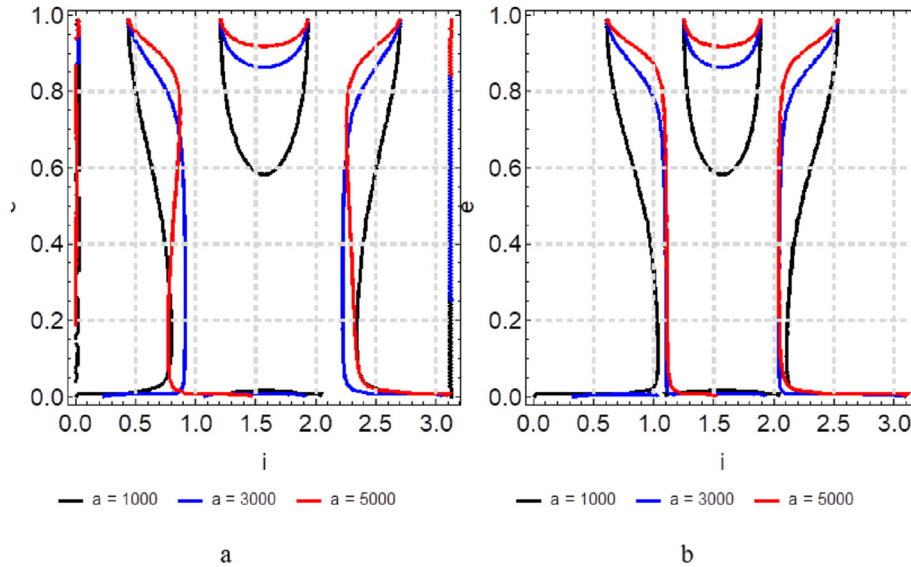


Fig. 1. The locations of frozen orbits in the (i, e) space for the two force models with different semi-major axes.

Figure 5 shows the long-term propagation of the eccentricity and inclination of the spacecraft using an averaged force model. The figure depicts the propagation under perturbation due to the complete force mode (red color), and model without a third body (black color). The initial conditions are $e = 0.75, i = 90^\circ, \omega = 90^\circ, \Omega = 90^\circ, M = 0^\circ, \beta = 0.024,$ and $a = 2000 \text{ m}$. The figure shows the shift in the curves due to the third-body perturbation. It is also observed that, in both models, the eccentricity and inclination oscillate with small amplitudes.

Figure 6 illustrates the time variation of the same orbital elements for different semi-major axes. The propagations are performed under full perturbations with initial conditions $e = 0.75, i = 90^\circ, \omega =$

$90^\circ, \Omega = 90^\circ, M = 0^\circ,$ and $\beta = 0.0237$. The figure shows the significance of changing the semi-major axis.

Figure 7 represents the time variation of the orbital elements for different β . The propagations are carried out under full perturbations with initial conditions $e = 0.75, i = 90^\circ, \omega = 90^\circ, \Omega = 90^\circ, M = 0^\circ,$ and $a = 2000 \text{ m}$. The figure shows that the effect of small β can be neglected, while for large values its effect is significant, particularly in the inclination.

Figure 8 illustrates the time variation of the orbital elements for different initial eccentricities. The force model includes the full perturbations. The initial conditions used are $i = 90^\circ, \omega = 90^\circ, \Omega = 90^\circ, M = 0^\circ, \beta = 0.0237,$ and $a = 2000 \text{ m}$.

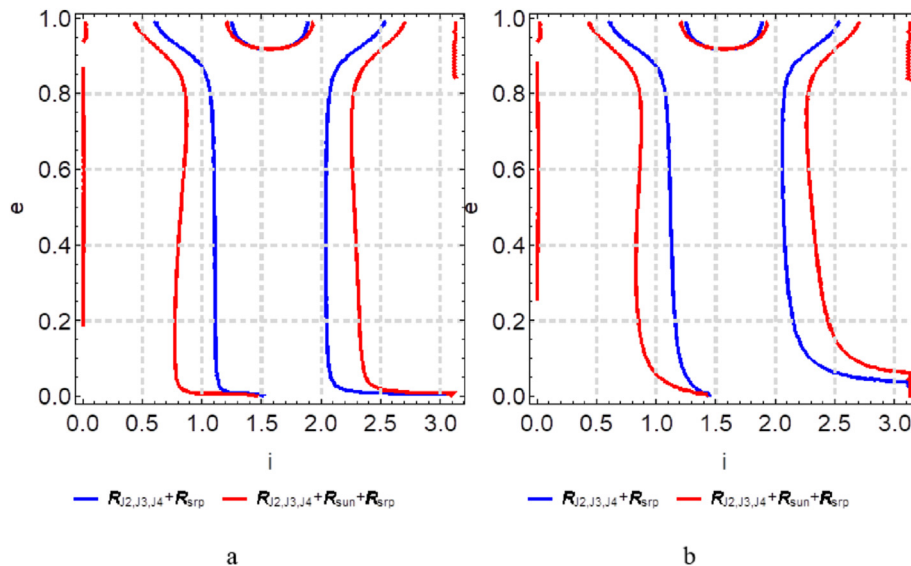


Fig. 2. The locations of the frozen orbits in the (i, e) space for different β .

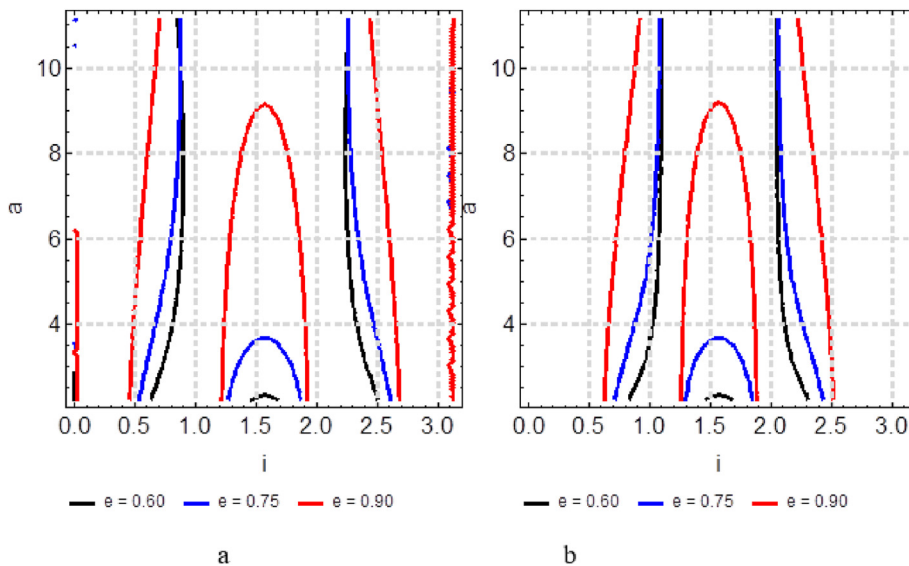


Fig. 3. The plan of the frozen orbit in the (a, i) space for different eccentricity values.

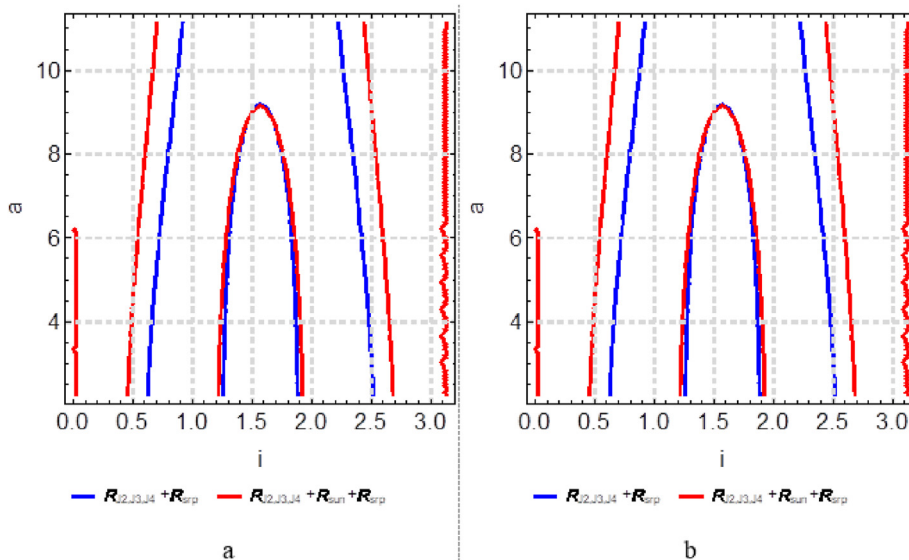


Fig. 4. The locations of the frozen orbits in the (a, i) space for different β .

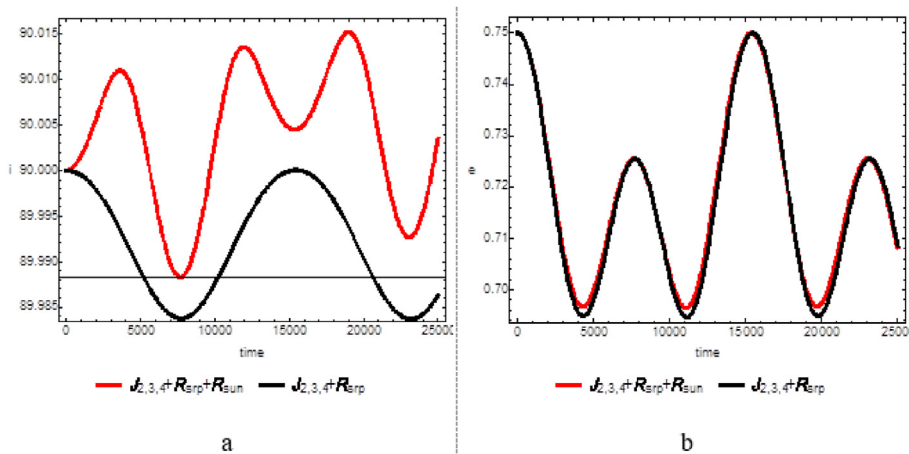


Fig. 5. The time variation of the inclination and eccentricity with two force models.

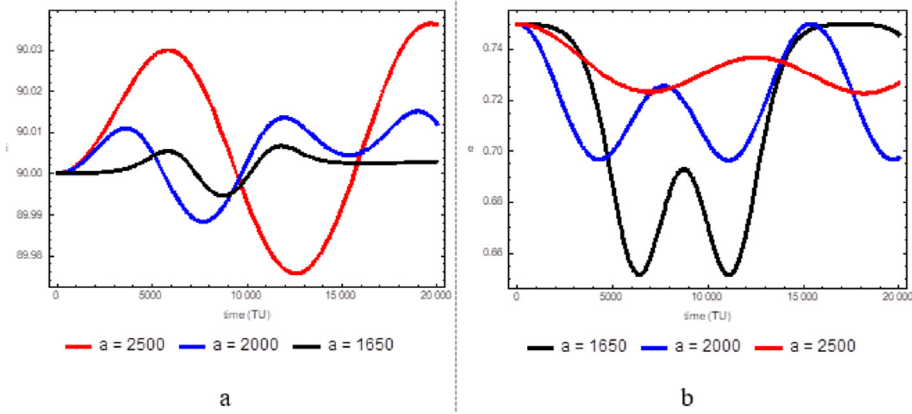


Fig. 6. The time variation of the inclination and eccentricity with different semi-major axis.

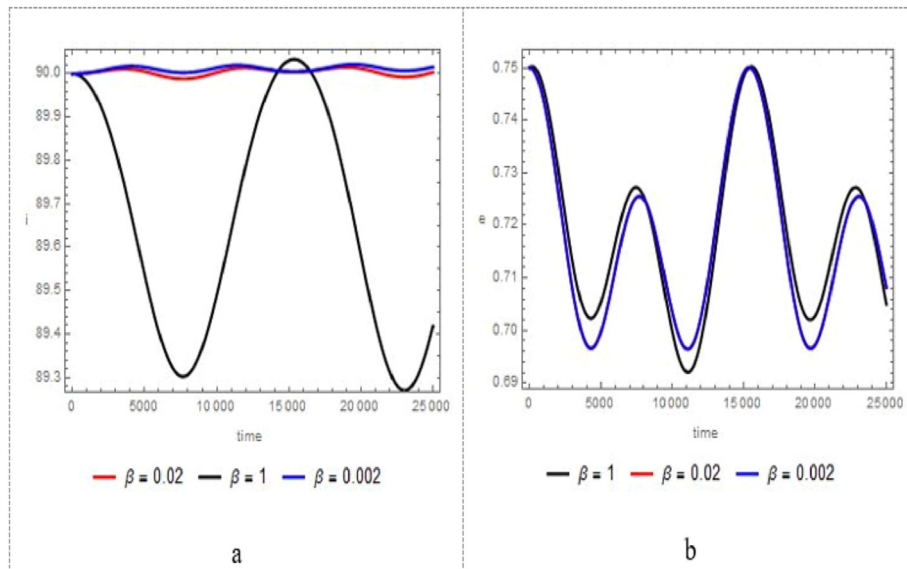


Fig. 7. The time variation of the inclination and eccentricity with different β .

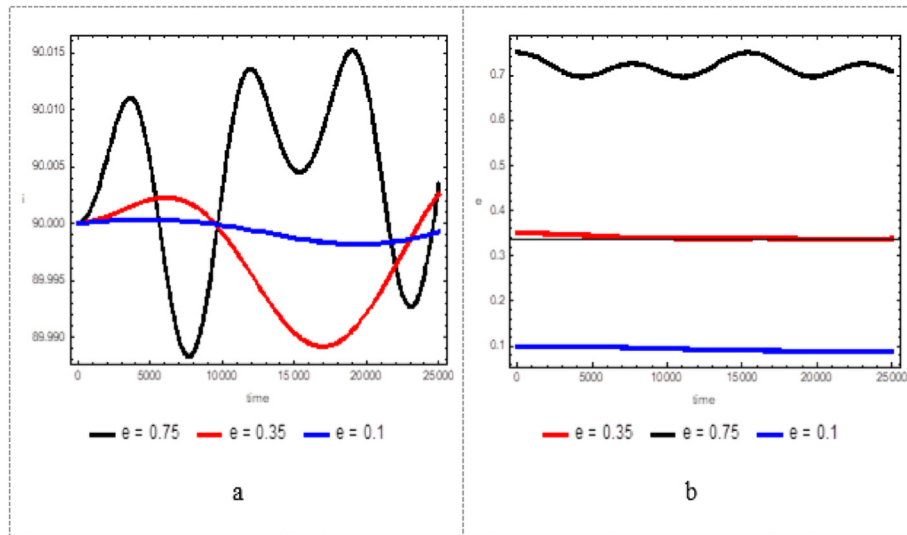


Fig. 8. The time variation of the inclination and eccentricity with different eccentricities.

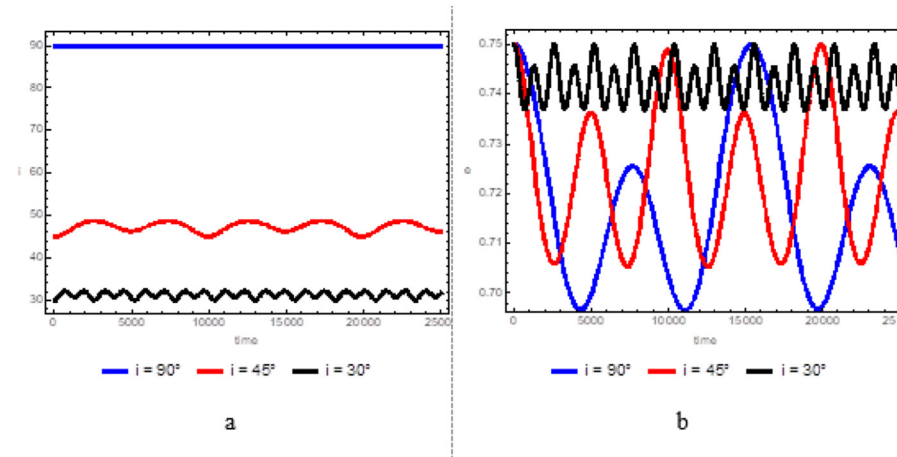


Fig. 9. The time variation of the inclination and eccentricity with different inclinations.

Figure 9 illustrates the time variation of the orbital elements for different initial inclinations. The force model contains the full perturbations. The initial conditions used are $e = 0.75$, $\omega = 90^\circ$, $\Omega = 90^\circ$, $M = 0^\circ$, $\beta = 0.0237$, and $a = 2000$ m. It is observed from Figs. 8 and 9 that the variations in both e , and i are close to their initial values.

5. Conclusion

Missions to asteroids encounter several dynamic challenges, such as the low-gravity environment of asteroids and strong perturbations due to SRP and a third-body attraction. To overcome this problem, frozen orbits around asteroids are a suitable solution.

In the present work, frozen orbits around the Ryugu asteroid are obtained under the effect of its gravitational field up to fourth order. In addition, the SRP and third-body attraction perturbations are considered. The third body shifts slightly the location of the frozen orbits. The dynamical behavior of the probe around Ryugu under the full model differs from that without a third-body attraction. Changing quantities like semi-major axis, inclination, etc. lead to a change in the location of the frozen orbits.

Funding sources

This research received no external funding.

Author contribution

M.R., A.A.A. and A.H.I. made conceptualization, visualization and formal analysis; M.R., A.A.A. and A.B. achieved investigation and methodology; M.R., A.A.A. and A.H.I. made software; A.A.A., M.R. and A.B., wrote the main manuscript text original draft. All authors certify that they have participated sufficiently in the work to take public responsibility for the content.

Conflict of interest

There are no conflicts to declare.

References

- [1] Scheeres DJ, Ostro SJ, Hudson RS, DeJong EM, Suzuki S. Dynamics of orbits close to asteroid 4179 Toutatis. *Icarus* 1998;132(1):53–79.
- [2] Utashima M. Spacecraft orbits around asteroids for global mapping. *J Spacecraft Rockets* 1997;34:226–32.
- [3] Ceccaroni M, Biggs J. Analytical perturbation method for frozen orbits around the asteroid 433 Eros. In: 63rd international astronomical congress; 2012.
- [4] Tresaco E, Elipe A, Carvalho JPS. Frozen orbits for a solar sail around Mercury. *J Guid Control Dynam* 2016;39:1659–66.
- [5] Takahashi S, Scheeres DJ. Higher-order corrections for frozen terminator orbit design. *J Guid Control Dynam* 2020; 43:1642–55.
- [6] Kikuchi S, Oki Y, Tsuda Y. Frozen orbits under radiation pressure and zonal gravity perturbations. *J Guid Control Dynam* 2021;44:1924–46.
- [7] Jiang Y, Baoyin H, Li H. Periodic motion near the surface of asteroids. *Astrophys Space Sci* 2015;360:1–10.
- [8] Jiang Y, Baoyin H. Periodic orbit families in the gravitational field of irregular-shaped bodies. *Astron J* 2016; 152:137.
- [9] Jiang Y, Baoyin H, Li J, Li H. Orbits and manifolds near the equilibrium points around a rotating asteroid. *Astrophys Space Sci* 2014;349:83–106.
- [10] Kanamaru M, Sasaki S, Morota T, Cho Y, Tatsumi E, Hirabayashi M, et al. YORP effect on asteroid 162173 Ryugu: implications for the dynamical history. *J Geophys Res: Planets* 2021;126(12):e2021JE006863.
- [11] Celletti A, Pucacco G, Vartolomei T. Proper elements for space debris. *Celestial Mech Dyn Astron* 2022;134:11.
- [12] Kaula WM. Theory of satellite geodesy, vol. 345. Waltham, Mass: Blaisdell Publ. Co.; 1966. p. 316.
- [13] Kaula WM. A development of the lunar and solar disturbing functions for a close satellite. *National Aeronautics and Space Administration* 1962;67:300.
- [14] Giacaglia GEO. A note on Hansen's coefficients in satellite theory. *Celestial Mech* 1976;14:515–23.
- [15] Jarnagin MP. Expansions in elliptic motion, *Astronomical papers of the American ephemeris and nautical almanac* Vol. 18. Washington: US Government Printing Office; 1966.
- [16] Brouwer D, Clemence GM. Methods of celestial mechanics. New York and London: Academic Press; 1961.